Numerical study of Rayleigh fission of a charged viscous liquid drop

Neha Gawande, Y. S. Mayya, and Rochish Thaokar
Indian Institute of Technology Bombay, Mumbai, Maharashtra 400076, India
(Received 18 March 2017; published 15 November 2017)

It is well known that a spherical drop charged beyond its Rayleigh limit becomes unstable (when subjected to a small shape perturbation) and ejects a significant fraction of the original charge in the form of a jet. To understand the detailed mechanism of this process, we model a charged drop of a perfectly conducting viscous liquid numerically using the boundary-element method. It is found from the simulations that the drop progressively deforms into a conical shape with pointed ends just prior to breakup. For ethylene glycol droplets suspended in air, the drop attains an aspect ratio of 3.86 at its critical shape, close to the observed value of 3.85 in the experimental images available in the literature. As the numerical approach fails to predict charge ejection due to the occurrence of a singularity at this point, the charge loss fraction is estimated by determining how much minimum charge must be removed if the drop is to relax back to a spherical shape. In this manner, the charge loss due to Rayleigh fission (the difference between the original charge and the minimum charge removed) is estimated to be about 39%, which falls within the range of experimental data lying between 20% and 50%. The results on scaling laws, time scales of the process, and the role of various stresses on the dynamics of the drop are discussed.

DOI: 10.1103/PhysRevFluids.2.113603

I. INTRODUCTION

The disintegration of charged water drops into fine droplets is a well-known natural phenomenon that occurs in thunderstorm clouds [1]. In recent times, the principle of disintegrating charged liquid drops has been utilized in various electrospray [2,3] based technologies such as aerosol generators for drug delivery [4], inkjet printing, microfluidic devices [5], and electrospray ionization mass spectrometry [6,7]. These developments have given considerable impetus in recent years [8–11] to the study of various mechanisms pertaining to the disintegration of electrified droplets. Lord Rayleigh [12] predicted that a charged conducting liquid drop of radius a develops instabilities and breaks up when its charge Q exceeds the limit

$$Q_R = 8\pi\sqrt{\epsilon\epsilon_0\gamma a^3}, \tag{1}$$

where Q_R is the critical charge γ, ϵ is the surface tension and dielectric constant of the liquid, respectively, and ϵ_0 is the permittivity of free space. Equation (1) represents the well-known expression for the Rayleigh limit. Rayleigh also stated that when $Q > Q_R$, the droplet would break up via the ejection of fine jets from its conical ends, leading to a loss of charge and mass. Although more than a century has passed since Rayleigh's predictions, several questions such as the sizes of the jets and precise knowledge of the pathway leading to their ejection, etc., still remain unanswered. Most importantly, the amount of charge lost in Rayleigh fission and its dependences on liquid properties have not been unequivocally established.

There have been several experimental efforts to validate the Rayleigh limit as well as to understand the breakup mechanisms. Doyle *et al.* [13] were among the first few to use Millikan's oil drop experimental setup to examine the stability of evaporating charged aniline and water droplets. Although the charge Q and mass m of the droplet were not estimated simultaneously, these authors pointed out the relation between sudden changes in the Q/m ratio and Rayleigh breakup. This study provided a charge loss of about 30% during the breakup, while a negligible mass loss was implicitly assumed in the process. Using an improved setup, Abbas and Latham [14] demonstrated successive breakup of an evaporating drop and estimated about 25% charge loss. Interestingly, their mass loss

estimate was also about 25%. In contrast, Schweizer and Hanson [15] observed a charge loss of about 25%, with a mass loss of about 5%.

Several other experimental studies reported a range of charge and mass losses. For example, using levitation techniques, Roulleau and Desbois [16] estimated a charge loss in the range of 16% – 40% but could not detect the mass loss. Taflin *et al.* [17] observed a charge loss of about 10%–18% and a mass loss of 1%–2.3%. Using electrodynamic balance for drop levitation, Richardson *et al.* [18] observed a 15% charge loss for dioctyl phthalate droplets and around 50% for sulfuric acid drops. The mass loss observed in the case of both the liquids was less than 2.5%. These results have been summarized succinctly by Shrimpton [19]. On the whole, experimental results estimate the charge loss in the range of 15%–50% with less than 5% mass loss (with the exception of those of Abbas and Latham). The discrepancy observed in different experiments may be attributed to the errors encountered in the measurements due to the very fast dynamics of the process as well as the influences of other parameters such as applied electric field, acceleration due to gravity, and aerodynamic drag.

More recently, direct visual evidence showing the instability and breakup of a charged drop was provided by the remarkable experiments of Duft *et al.* [1], which combined electrodynamic levitation techniques with synchronized high-resolution time-elapsed photography. They reported the charge loss in the breakup process to be 33% and the mass loss less than 1%. The sequence of images of drop deformation and breakup reported by these authors triggered quite a few analytical and numerical studies aimed at understanding this phenomenon [20–25]. These studies numerically investigated the dynamics of breakup of a charged droplet using axisymmetric boundary-element method in the limit of either viscous flow [20] or potential flow regimes [21,23]. Moreover, two studies addressed the problem with finite-Reynolds-number formulation [22,24], using the finite-element method. The phenomenon of Rayleigh breakup can be described in three stages, which include drop deformation into an elongated shape having sharp conical tips, ejection of a jet from these tips, and subsequent relaxation of the deformed drop back to the spherical shape. It is a challenging task to trace all these stages through a single computational formalism as the numerical codes break down particularly due to the formation of shape singularity at the tip. This difficulty is often circumvented by examining the progressive and regressive stages separately and invoking analytical insights pertaining to their behavior near the shape singularities. Towards this end, Betelú *et al.* [20] introduced the use of scaling laws to describe shape evolution near the sharp conical tips. This was a major development in the understanding of the instability of charged drops. A similar study was reported by Burton and Taborek [21], focusing on the progressive deformation of the drops until the stage of formation of conical tips, beyond which the numerical algorithms break down due to the occurrence of singularities.

Interestingly, Giglio *et al.* [25] reported a study of charged drops combining numerical analysis with experiments, which included both progressive and relaxation regimes. Though the numerically obtained shapes for progressive regime were in general agreement with the experiments, relaxation back to a spherical shape was not observed due to the absence of viscous damping in the model. In another study, Radcliffe [24] correctly predicted the drop relaxation to the spherical shape by including viscous effects through finite-Reynolds-number methodology. However, in his formulation, the charge on the drop surface was arbitrarily reduced by assuming a 40% charge loss from the drop. Garzon *et al.* [23] used the boundary-element method (BEM) combined with level set method to study the actual ejection of the Rayleigh jets. Though the time scales of deformation are in good agreement with the experiments of Giglio *et al.* [25], the relaxation to a spherical shape was not observed again due to noninclusion of the viscous effects. Their study also overpredicted the charge loss (of about 50%) in the Rayleigh fission of supercooled water drops as compared to experiments (30%).

From the discussion above it is clear that, while past studies have mainly focused on the evolutionary dynamics of the droplet, the question of charge lost during Rayleigh fission has essentially remained open. This fact forms the primary motivation for the present study. We attempt to estimate the fraction of charge ejected by a drop by exploring both its progressive and regressive dynamics, separately, within the framework of the viscous flow BEM. The justification for using the

viscous flow regime stems from the following arguments. From the experimental images of Giglio *et al.* [25], a typical velocity of the process is seen to be about 0.5 m/s, which yields a low Reynolds number of about 1 (for an ethylene glycol drop in air) at which viscous stresses will dominate over inertial stresses, overwhelmingly. Furthermore, we note that after the ejection of the jet, the drop relaxes back into the shape of a sphere rather smoothly, in a nonoscillatory manner, which is a definite characteristic of an overdamped system. This points to the fact that the viscous flow model is better suited to capture the overall dynamics of the charged drops.

However, the breakdown of the numerical algorithm near the jet ejection stage makes it difficult to predict the charge loss directly. To circumvent this problem, we use a strategy originally proposed by Giglio *et al.* [25] in which the regression dynamics is examined separately by systematically removing the charge from the deformed drops. The charge lost Q_L during fission is then postulated as

$$Q_L = Q_R - Q_c, \tag{2}$$

where Q_c is the maximum critical charge required by a maximally deformed drop (just before Rayleigh fission) to relax back to the spherical shape, without any ejection. The corresponding mass loss may be argued to be negligible, in line with the observed experimental values. The time of occurrence of singularity and the corresponding shapes are ascertained by seeking conformity of the numerical results with the scaling laws of Betelú *et al.* [20] through best-fit analyses. The approach not only improves our understanding of the interplay between the electric, capillary, and viscous stresses acting on the drop, but also leads to a unique estimate of the charge lost during Rayleigh fission.

II. PROBLEM FORMULATION

We consider a perfectly conducting liquid drop of radius a, carrying an electric charge Q, suspended in a dielectric Newtonian fluid medium. The various parameters corresponding to the drop and external medium are denoted by subscripts i and e, respectively. Thus μ_i (μ_e), ϵ_i (ϵ_e), and $\tilde{\phi}_i$ ($\tilde{\phi}_e$) denote the viscosity, dielectric constant, and electric potential of the drop (external medium), respectively. The interfacial tension between the two fluids is denoted by γ. The induced electric field in the respective domains is expressed via the relation $\tilde{\mathbf{E}} = -\tilde{\nabla}\tilde{\phi}$. Given the insulating nature of the perfectly dielectric external fluid medium, the total charge on the conducting drop surface remains constant during deformation. Hence Gauss's law is used to impose conservation of charge on the equipotential drop surface. The charge density at the surface of the drop is given by the difference in the electric displacements between the external and internal media

$$\tilde{q} = \epsilon_0\epsilon_e \mathbf{n}\cdot(-\tilde{\nabla}\tilde{\phi}_e) - \epsilon_0\epsilon_i \mathbf{n}\cdot(-\tilde{\nabla}\tilde{\phi}_i) = \epsilon_0\epsilon_e \tilde{E}_{ne}, \tag{3}$$

where $\mathbf{n}$ is the outward unit normal and $\tilde{E}_{ne}$ is the normal component of the externally directed electric field ($\tilde{E}_{ni} = 0$, since the drop is assumed to be a perfect conductor). As stated in the Introduction, the Reynolds numbers associated with the deformation process are considerably small and hence we may neglect the inertial effects and treat the problem within the framework of the viscous formulation (Stokes flow). The Stokes equation for the flow field and the Laplace equation for the electric potential are solved simultaneously using the boundary-element method.

A. Governing equations

The electrostatic equations for the electric fields $\tilde{E}_{i,e}$ and electric potentials are given as

$$\tilde{\nabla}\cdot\tilde{\mathbf{E}}_{i,e} = 0 \quad \text{or} \quad \tilde{\nabla}^2\tilde{\phi}_{i,e} = 0, \tag{4}$$

whereas the continuity and the Stokes equation relating the velocity fields $\tilde{v}_{i,e}$ to pressure fields $\tilde{p}_{i,e}$, are given as

$$\tilde{\nabla}\cdot\tilde{\mathbf{v}}_{i,e} = 0, \tag{5}$$

$$-\tilde{\nabla}\tilde{p}_{i,e} + \mu_{i,e}\tilde{\nabla}^2\tilde{\mathbf{v}}_{i,e} = 0. \tag{6}$$

Dimensional quantities are indicated by a tilde. The bold symbols indicate vector quantities. With these, the force balance at the interface is given by

$$\mathbf{n}\cdot\left(\tilde{\tau}_e^H-\tilde{\tau}_i^H\right)+\mathbf{n}\cdot\left(\tilde{\tau}_{\mathbf{e}}^{\mathbf{E}}-\tilde{\tau}_i^{\mathbf{E}}\right)-\gamma\mathbf{n}(\tilde{\nabla}_s\cdot\mathbf{n})=0, \tag{7}$$

where $\tilde{\tau}$ is the hydrodynamic stress, $\tilde{\tau}^E$ is the Maxwell electric stress tensor γ, and $\tilde{\nabla}_s\cdot\mathbf{n}$ are the surface tension and curvature, respectively. Equation (7) represents the balance between viscous stresses, capillary forces, and electric stresses. These stresses in turn are related to the field variables as follows: The electric stress tensor

$$\tilde{\tau}^{\mathbf{E}}=\epsilon\epsilon_0\left[\tilde{\mathbf{E}}\tilde{\mathbf{E}}-\tfrac{1}{2}\mathbf{I}(\tilde{\mathbf{E}}\cdot\tilde{\mathbf{E}})\right] \tag{8}$$

and the hydrodynamic stress tensor

$$\tilde{\tau}^H=-\tilde{p}\mathbf{I}+\mu[\tilde{\nabla}\tilde{\mathbf{v}}+(\tilde{\nabla}\tilde{\mathbf{v}})^T]. \tag{9}$$

The following nondimensionalization is used to scale the flow parameters: Lengths are scaled by a (drop radius), velocities by $\frac{\gamma}{\mu}$, time by $\frac{\mu_e a}{\gamma}$, stresses by $\frac{\gamma}{a}$, electric fields by $\sqrt{\frac{\gamma}{a\epsilon_e\epsilon_0}}$, and charges by $\sqrt{\gamma a^3\epsilon_e\epsilon_0}$. Accordingly, the nondimensional Rayleigh charge limit (1) will be $Q_R=8\pi$. In terms of scaled variables, the nondimensional electrohydrodynamic equations may be written as

$$\nabla\cdot\mathbf{v}_{i,e}=0, \tag{10}$$

$$-\nabla p_{i,e}+\chi_{i,e}\nabla^2\mathbf{v}_{i,e}=0, \tag{11}$$

where $p_{i,e}$ is the pressure, $\chi_e=1$ for the external medium, $\chi_i=\lambda=\mu_i/\mu_e$ inside the drop, and

$$\nabla^2\phi=0. \tag{12}$$

In the BEM, the governing equations are transformed into integral representations for ϕ and v. Upon using the Gauss divergence theorem, the volume integrals are converted into surface integrals and the azimuthal parts of the surface integrals are analytically integrated out using axisymmetric assumption. With this, the integral equation for the electric potential ϕ is given as

$$\phi(\mathbf{r}_s)=\int\frac{E_{ne}(\mathbf{r})}{|\mathbf{x}|}dS(\mathbf{r}), \tag{13}$$

where $\mathbf{x}=(\mathbf{r}-\mathbf{r}_s)$ and $\mathbf{r}_s$ represents a point on the drop surface where the electric field or velocity is being calculated while $\mathbf{r}$ is the integration variable. Equation (13) is solved simultaneously with the following nondimensional equation for the conservation of total charge Q on the drop surface to determine the nondimensional charge density q $(=E_{ne})$ and the surface potential ϕ:

$$\int q(\mathbf{r})dS(\mathbf{r})=\int E_{ne}(\mathbf{r})dS(\mathbf{r})=Q. \tag{14}$$

The integral equation for the interfacial velocity is given by

$$\begin{aligned}\mathbf{v}(\mathbf{r}_s)=&-\frac{1}{4\pi(1+\lambda)}\int\triangle\mathbf{f}(\mathbf{r})\cdot\mathbf{G}(\mathbf{r},\mathbf{r}_s)dS(\mathbf{r})\\&+\frac{1-\lambda}{4\pi(1+\lambda)}\int\mathbf{n}(\mathbf{r})\cdot\mathbf{T}(\mathbf{r},\mathbf{r}_s)\cdot\mathbf{v}(\mathbf{r})dS(\mathbf{r}).\end{aligned} \tag{15}$$

Here $\mathbf{G}(\mathbf{r},\mathbf{r}_s)=\frac{\mathbf{I}}{|\mathbf{x}|}+\frac{\mathbf{xx}}{|\mathbf{x}|^3}$ and $\mathbf{T}(\mathbf{r},\mathbf{r}_s)=-6\frac{\mathbf{xxx}}{|\mathbf{x}|^5}$ are the kernel functions and the traction across the interface is

$$\Delta f=\left(\nabla_s\cdot\mathbf{n}-\tfrac{1}{2}E_{ne}^2\right)\mathbf{n}, \tag{16}$$

where $\nabla_s \cdot \mathbf{n}$ represents curvature of the drop surface and $\frac{1}{2}E_{ne}^2$ is the electrical stress calculated for the given total charge Q. Here $\mathbf{n}$ is the outward unit normal to the surface of the drop. The detailed derivation of these integral equations and the origin of the kernels have been extensively discussed in the literature [26,27].

B. Numerical scheme

The half contour of the surface of the drop is uniformly discretized into 300 elements and all the functions are interpolated by parametric cubic splines with respect to arc length s. The integral equations are discretized and the system of equations is solved by the LU decomposition method. An initial charge of $Q = 8.1\pi$, which is a little over 1% of the nondimensional Rayleigh charge 8π, is placed on the droplet surface to initiate deformations. However, a perfect sphere does not undergo deformation spontaneously even if it charged beyond Rayleigh limit [28]. Hence, a small shape deformation is introduced initially via a function of the form $r(\theta) = a\{1 + \delta P_2[\cos(\theta)]\}$, where $\delta \ll 1$ is a small amplitude of perturbation and $P_2[\cos(\theta)]$ is the second-degree Legendre polynomial. The surface charge density on the drop is then calculated using Eqs. (13) and (14). The Maxwell stresses are evaluated using a normal electric field and from this the traction force is evaluated using Eq. (16). The drop undergoes deformation due to an imbalance between the electric and capillary forces. The interfacial velocity is then obtained from Eq. (15) and the node points are advanced using the Euler method,

$$\mathbf{r}_s^{t+1} = \mathbf{r}_s^t + \mathbf{v}(\mathbf{r}_s)\triangle t. \tag{17}$$

The simulations are carried out until the numerical scheme breaks down, which occurs at the onset of shape singularity of the drop. Although the numerical algorithm followed is similar to those used in the earlier studies [29,30], the number of elements used here is significantly larger than those previously employed, thereby increasing the accuracy of our calculations. It was observed that the use of uniformly distributed node points yields a small neck at the poles of the elongated drop; however, the length of this neck was found to be inversely proportional to the number of elements in which the drop was discretized. This observation indicated a need for higher resolution in the tip region, which in turn demanded higher computational time. In order to increase the resolution near the poles without unduly increasing the computational time, a nonuniform grid structure, more closely spaced at the poles than at the equatorial region, was used. With an optimum number of elements, one could achieve a smooth evolution of the tip into a conical shape without forming a neck. Thus, neck formation appears to be a numerical artifact and should be interpreted with caution. The numerical calculations tend to become unreliable beyond the critical shape corresponding to the onset of jet ejection after which the charge density and the curvature at the tip start diverging in time. The nondimensional time step is then reduced by a factor of 100 as the singularity is approached. The time at which the singularity occurs, the critical shape, and the corresponding aspect ratio are then obtained by fitting the numerical data to self-similar solutions where the aspect ratio (AR) $\mathcal{A}$ is defined as

$$\mathcal{A} = \frac{r_s(\theta = 0)}{r_s(\theta = \pi/2)}. \tag{18}$$

To study the drop relaxation dynamics, one starts with a critically deformed shape and progressively reduces its charge until it starts to relax back towards the original spherical shape. In this regime, simulations are carried out until the tip velocity becomes negligibly small [$O(10^{-5})$] and the shape becomes spherical. All computations are performed in FORTRAN 77 using double-precision data type. As the jet ejection is not directly considered here, there will be no loss of mass. As a result, volume conservation is ensured to an accuracy of 0.1% of the original volume in all the simulations.

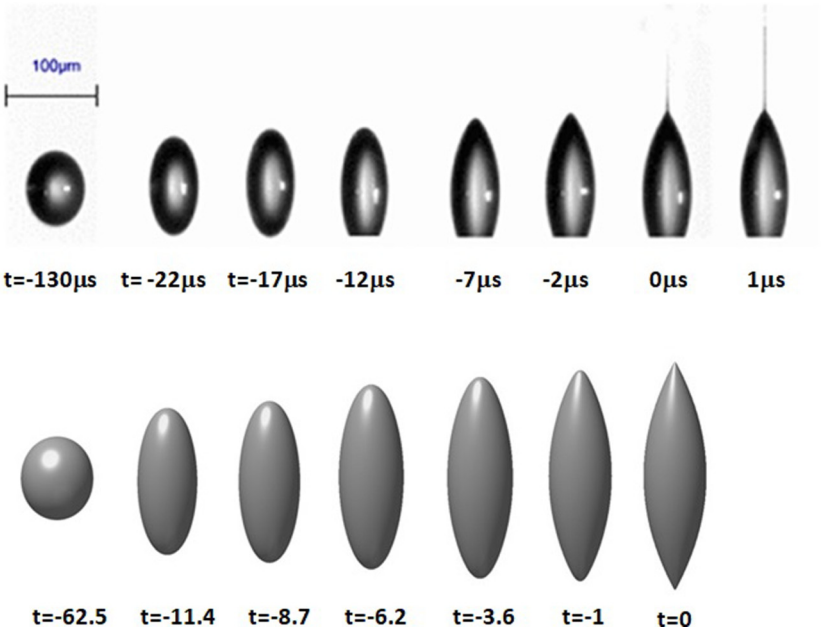

FIG. 1. Comparison of the experimental observations of evolution of drop shapes reported by Giglio *et al.* [25] (top) with the present simulations (bottom). The simulations are carried out starting with a prolate spheroid of eccentricity $\delta = 0.1$, charge $Q = 8.1\pi$, and $\lambda = 1$ until a point in time when the conical tips develop. The times shown for the simulations are nondimensional reckoned with respect to the time (zero) for the occurrence of the critical shape.

III. RESULTS AND DISCUSSION

We first consider the progress of deformation of a drop initially charged to 8.1π and subjected to a small shape deformity, as mentioned earlier. The sequence of deformation states of such a drop obtained from simulations corresponding to viscosity ratio $\lambda = 1$ is presented in Fig. 1. It can be seen that the drop evolves progressively into a shape forming sharp conical ends at the poles. It is expected that the sharpening of the tips would continue until a critical time (occurring at $\sim$62.5 units since the initial spherical shape, discussed later in Fig. 3) at which the jet ejection would take place. The corresponding shape may be referred to as a critical shape. These aspects are similar to those seen in the experiments of Giglio *et al.* [25]. The shape evolution is caused by the dominance of the outward-directed electric stresses over the capillary and the hydrodynamic stresses, all rapidly changing with time. The streamline plots of the velocity field inside and outside the drop surface (Fig. 2) show the signatures of extensional flow, common in a force dipole system. It is observed that as the time approaches the critical time the fluid inside the drop starts decelerating in the equatorial region while rapidly accelerating at the poles. This counterplay between the flow directions within and outside the drop indicates that the drop will eventually undergo tip streaming and relax back due to the stabilizing effect in the equatorial region. The red arrows shown in the figure indicate the relative magnitude of the normal electrical stresses acting on the surface of the drop. It can be seen that the electrical stress at the tip progressively becomes much higher than that at the equatorial region as the drop shape becomes increasingly sharper at the ends.

The shape evolution observed during the progressive stage prior to breakdown of the code may be quantitatively compared with experimental images of Giglio *et al.* [25]. Since the experiments correspond to an ethylene glycol–air system having a viscosity ratio of about 150 (at 85 °C), we performed separate simulations for the case of $\lambda = 150$. Giglio *et al.* [25] presented eight images in a span of 130 μs, six of which occur prior to the onset of ejection with the other two corresponding to

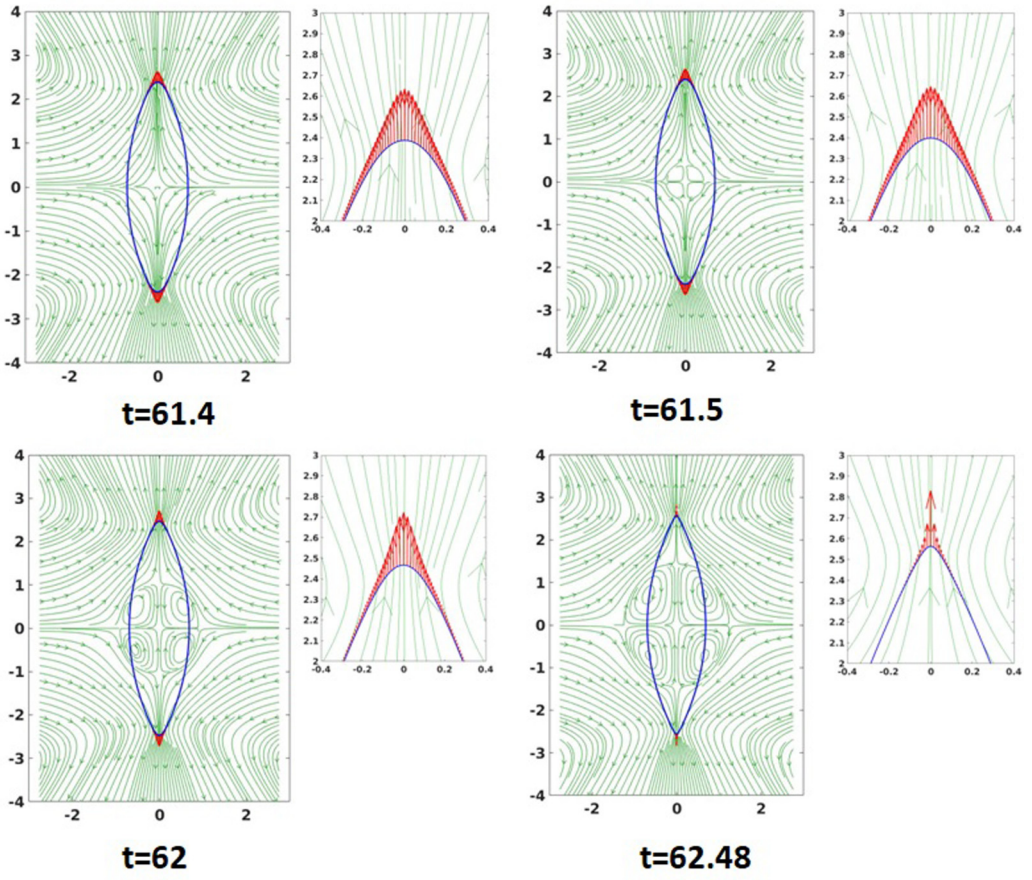

FIG. 2. Streamline plots of the drop near singularity. Green lines indicate the direction of fluid flow and red arrows correspond to the direction and relative magnitude of the electrical stresses acting on the drop surface along the arc length. The insets show focused tips of the corresponding shapes.

the onset and peak ejection events. In our simulations, the time to reach the singularity works out to be 45 μs (for $\lambda = 150$). In Fig. 3 we show a plot of the $\mathcal{A}$ values as a function of respective normalized times (by dividing the time to reach a given $\mathcal{A}$ with the maximum time to reach singularity) for both the experimental case and the simulations. For further comparison, cases of $\lambda = 1600$ (ethylene glycol–air system at 25 °C) and $\lambda = 1$ are also shown in Fig. 3. The $\mathcal{A}$ values obtained from the three simulations ($\lambda = 1$, 150, and 1600) are all close to each other (the curves for $\lambda = 150$ and $\lambda = 1600$ merge indistinguishably with each other). Interestingly, experimental values are distinctly lower than those predicted by simulations at intermediate normalized times and catch up with the latter as the normalized time approaches unity. This hints at the possibility that the inertial effects, neglected in our simulations, play a definite role in the intermediate dynamics of deformation. The maximum $\mathcal{A}$ obtained in the experiment is 3.85, which compares well with the $\mathcal{A}_{\max}$ values of 3.86 for $\lambda = 150$. The simulations show that the $\mathcal{A}_{\max}$ values vary marginally from 3.76 for $\lambda = 1$ to 3.9 for $\lambda = 1600$. These observations indicate that the inertial effects and the viscosity ratio λ only affect the deformation dynamics but not the critical shape attained by the drop. Hence, insofar as the assessment of the shape of the drop is concerned, neglecting inertial effects and assuming $\lambda = 1$ in computations is quite adequate. In view of this, subsequent studies on the relaxation of the droplet in the postejection phase were carried out for the numerically simpler case of $\lambda = 1$.

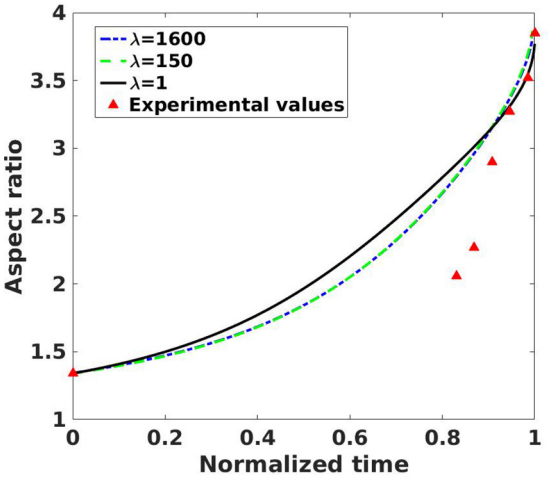

FIG. 3. Variation of aspect ratio with respect to self-normalized time for the three cases $\lambda = 1$, 150, and 1600 and their comparison with the experimental results reported by Giglio *et al.* [25]. The curves for $\lambda = 150$ and $\lambda = 1600$ overlap and thus cannot be distinguished.

It is observed that a drop approaches the singular shape in a finite time t_0, reckoned from the beginning of its deformation from the spherical shape. However, the breakdown of the numerical code (mentioned in the preceding section) near singularity makes it almost impossible to estimate t_0 directly. This limitation may be overcome by judiciously combining the numerical results with the available analytical scaling laws [20]. The self-similar solutions to describe the shape of the surface are expressed in the form

$$\frac{z_{\text{tip}} - z}{(t_0 - t)^{\alpha}} = f\left[\frac{r}{(t_0 - t)^{\alpha}}\right], \tag{19}$$

where (r,z) are the coordinates on the surface, z_{tip} is the coordinate of the tip, t_0 is the time of occurrence of singularity, α is the exponent $(0 < \alpha < 1)$, and f is an invariant shape function of r with respect to t. From Eq. (19), the curvature κ, charge density q, and velocity v at the tip will scale as

$$\kappa \sim (t_0 - t)^{-\alpha}, \tag{20}$$

$$q \sim (t_0 - t)^{-\alpha}, \tag{21}$$

$$v \sim (t_0 - t)^{\alpha - 1}. \tag{22}$$

It follows from Eqs. (20)–(22) that the hydrodynamic stress will scale as $dv/dr \sim (t_0 - t)^{-1}$ and the corresponding electrical stress $q^2 \sim (t_0 - t)^{-2\alpha}$. Using a combination of the numerical fit and analytical arguments, Betelú *et al.* [20] obtained the value $\alpha = 1/2$. Then the curvature, charge density, and velocity would scale as $(t_0 - t)^{-1/2}$ and the electrical and hydrodynamic stresses will scale as $(t_0 - t)^{-1}$. Since the capillary stress is proportional to curvature, it would scale as $(t_0 - t)^{-1/2}$. Thus, the capillary stresses become subdominant near the singularity $(t = t_0)$ and the shape is sustained solely by the hydrodynamic and electrical stresses.

Equation (19) can also be interpreted as implying that the shape is invariant when the (r,z) coordinates are scaled in terms of the radius of curvature of the tip. This is demonstrated in Fig. 4(b), wherein the shapes of the drop near the tip collapse onto a single curve in the scaled variables, for

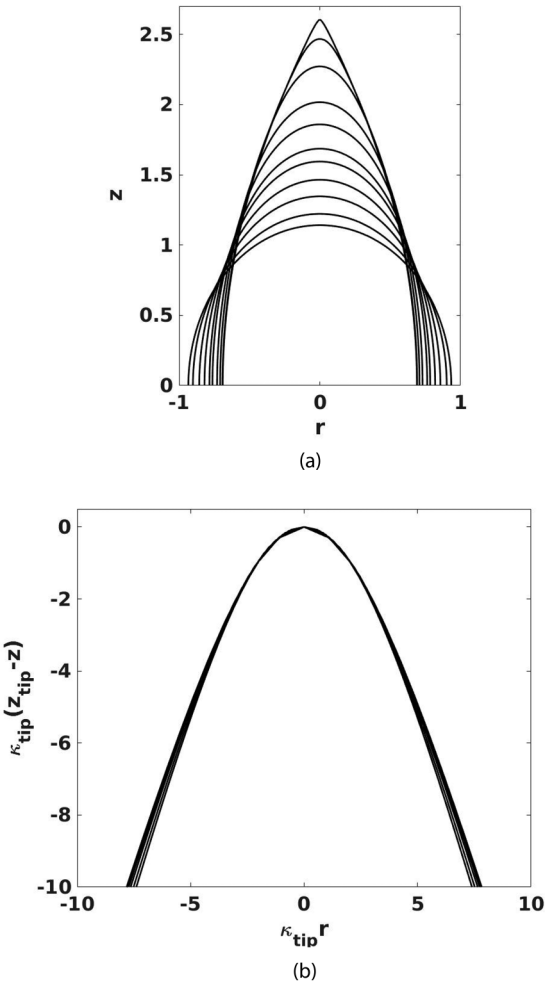

FIG. 4. (a) Profiles showing evolution of the drop surface with respect to time leading to formation of the conical tip. (b) Drop profiles rescaled to show the self-similarity of the shapes obtained with respect to nondimensional times 62.3, 62.4, 62.42, 62.45, 62.46, 62.47, and 62.48. The tip curvatures used for scaling corresponding to times are 51.494, 76.762, 88.01, 117.66, 134.78, 159.41, and 197.38, respectively.

the nondimensional times up to 62.48. Figure 4(a) shows the shape evolution of the drop near the tip with respect to time, in real (r,z) coordinates.

The drop approaches the shape of a cone near the tip, resembling the classical Taylor cone, as the point of singularity is approached at $t = t_0$. The semivertical angle of this cone is found to be 24.7° (Fig. 5), which is close to the result (25°) of Betelú *et al.* [20], although far lower than the Taylor cone angle (49.3°). This may be attributed to the subdominant capillary stresses. On the other hand, for the case of inviscid drops, a semiangle of 49.3°, similar to a Taylor cone, at the time of the onset of jet ejection was reported [21,23]. The experiment of Duft *et al.* [1] seems to yield a value of 33°, which is closer to our simulations (viscous drop assumption) rather than that corresponding to inviscid assumptions.

The time t_0 of occurrence of singularity is estimated as follows. Given the fact that the code is more accurate at times far from the singularity and the scaling laws are more accurate near the singularity, there will be an overlap region where both the scaling laws and the numerical results

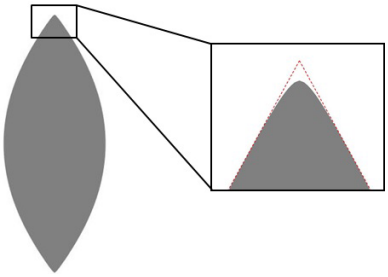

FIG. 5. Focused tip of the drop at a time just before the critical time t_0. It is observed that, near the tip, the drop surface is closely enveloped by a cone of semivertical angle of 24.7°.

should reliably agree with each other. To identify this region we examine the scaling behavior of the numerical data for the quantities such as curvature, charge density, and velocity, all computed at the tip, by applying a nonlinear curve fitting algorithm to a function of the form

$$y = A(t_0 - t)^{\alpha}, \tag{23}$$

where A, t_0, and α are fitting parameters. First, a time domain of the numerical data (excluding the too proximal and the too distal regions from the breakdown point) is selected. Then the power-law scaling exponents obtained from the best fit to the numerical data in this domain are compared with the analytical theory. By continually varying the data domain, one could arrive at the "best of the best fits" having the highest value for the correlation coefficient. The scaling obtained this way from the numerical data is shown in Fig. 6. The exponents obtained for curvature, charge density, and velocity were -0.51, -0.50, and -0.51, respectively, which are quite close to the theoretical values. The corresponding t_0 values were close to each other (differing only in the third decimal place), having an average of 62.5 ± 0.005. Hence, for the relaxation analysis (see below), a value of $t_0 = 62.5$ was taken as the best estimate of the time to reach the singular point (for $\lambda = 1$).

The following strategy is adapted for predicting the impending charge loss at the critical time t_0, around which the numerical method breaks down. It may be noted from the simulations that while a spherical drop requires a charge of at least 8π to undergo deformation following a small perturbation, an already elongated drop deforms further for charges less than 8π. A little reasoning shows that for a given shape deformation, there should exist a characteristic charge above which the drop will deform further and below which it will regress to a spherical shape. Seen from this perspective, a drop charged beyond its Rayleigh limit, upon deforming to its critical shape, would eject an amount of charge that will just be sufficient to cause the drop to regress towards a spherical shape. Alternatively, the residual charge after ejection will render the local electrical stress around the tip region to a level just below the capillary stress. Therefore, the difference between the initial charge and the residual charge at which a maximally deformed drop begins to regress should be the charge loss due to Rayleigh fission.

Based on the above reasoning, we perform simulations on the evolution of drops starting with different ARs (Fig. 7). For each of these ARs, the charge carried by the drop is decreased gradually from 8.1π until a level at which the drop reverses its direction of evolution (from the state of unstable deformation to regression towards a stable spherical shape). For example, for the drop representing a singular shape with the lowest AR ($\mathcal{A} = 3.676$) we find that it tends to deform further for all charges $Q > 5.78\pi$, whereas for $Q < 5.78\pi$ the drop regresses to the spherical shape (Fig. 8). Hence $Q_c = 5.78\pi$ is the maximum charge that the shape with $\mathcal{A} = 3.676$ can hold without becoming unstable. As the AR increases, this charge comes down; a shape with $\mathcal{A} = 3.744$ that is a short time away from reaching the singular point (Fig. 7) can hold a maximum charge of $Q_c = 5.1\pi$. A best-fit analysis to the sequence of data on $\mathcal{A}$ versus Q_c data yields a maximum charge $Q_c = 4.96\pi$ for the critical shape with $\mathcal{A} = 3.762$ (corresponding to the singular point) above which it would

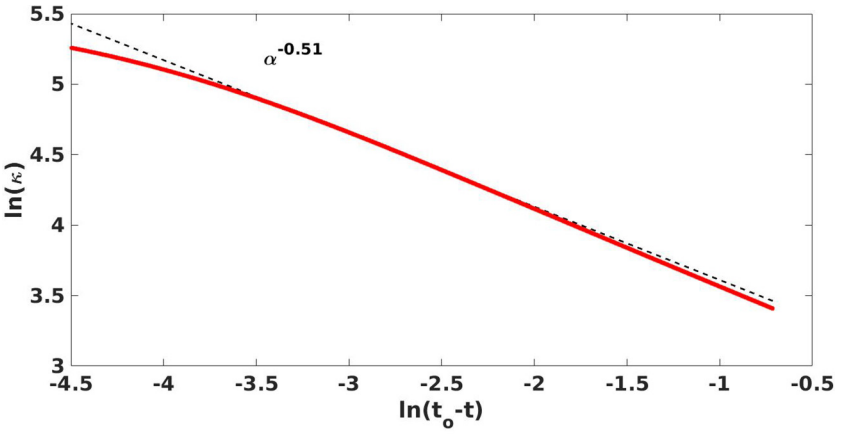

(a)

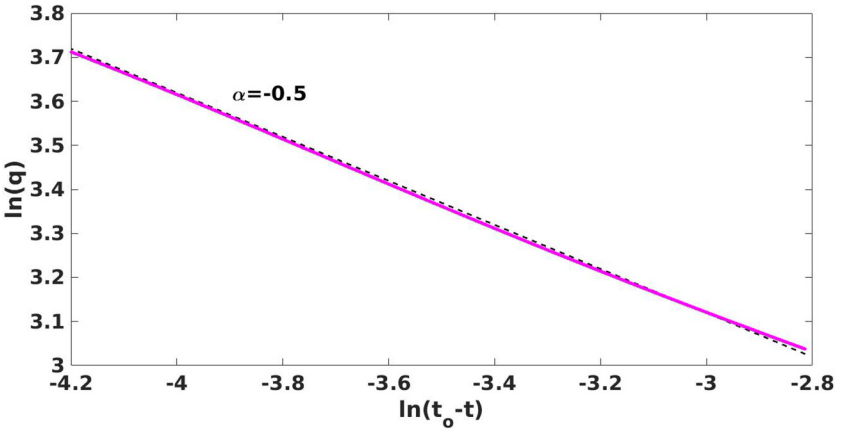

(b)

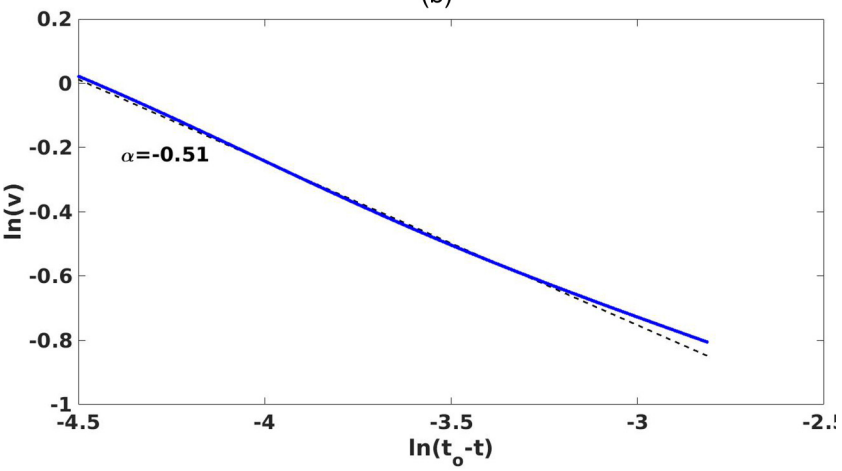

(c)

FIG. 6. Plots of (a) curvature κ, (b) charge density q, and (c) velocity v of the drop tip as a function of time obtained from the simulations with their corresponding best-fitted exponents.

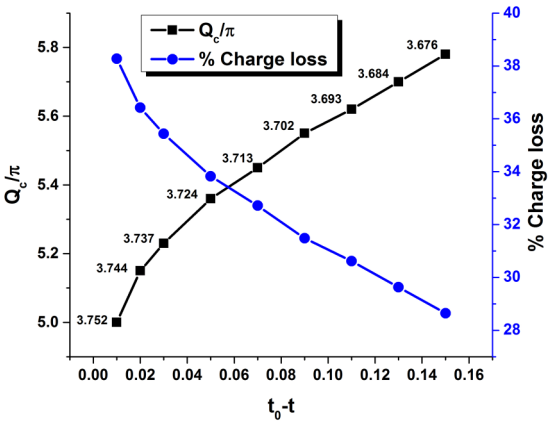

FIG. 7. Charge at which a deformed drop relaxes back to spherical shape as a function of time at which the critical shape of the drop is frozen and charge is reduced sequentially until the drop relaxes back to a sphere. The left-hand y axis indicates the scaled charge Q_c/π and the right-hand y axis shows the percentage of charge lost in the process. The numbers shown indicate the aspect ratio of the drop shape for the corresponding time.

be unstable. Thus 4.96π may be considered to be the charge retained by the drop after ejecting the excess charge. From the difference between the initial charge (8.1π) and Q_c ($=4.96\pi$), we estimate the charge loss to be 3.14π, which constitutes about a 39% charge loss. Since this charge is ejected from a small region around the tip of the deformed drop, the ejected mass can indeed be considered very small. A heuristic estimate of this quantity may be made as follows. Assume a conical shape with slant height l_m for each side of the deformed drop. For a conducting surface, the charge density varies as $\sim l^{(\nu-1)}$ [31] with respect to the slant distance l from the tip (where ν is a positive number less than 1). The cumulated charge fraction f_c will then be $f_c = (l/l_m)^{\nu+1}$ and the corresponding mass fraction will be $f_m = (l/l_m)^3 = f_c^{3/(\nu+1)}$. For extremely sharp tips, $\nu \sim 0$ and we get $f_m = f_c^3$. Thus, for $f_c = 40\%$, this estimate yields $f_m = 6.4\%$–7%. This calculation justifies, *a posteriori*, the assumption of negligible mass loss made in the simulations. As this assumption is also borne out in experiments, the simulations show an overall consistency with them with respect to significant charge loss and negligible mass loss. Although the results presented here pertain to a case

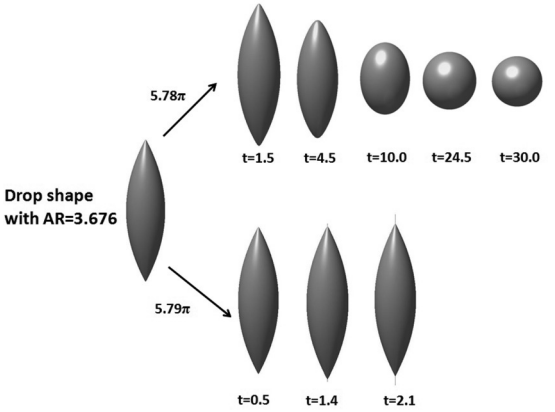

FIG. 8. Evolution of the drop in the relaxation regime from the shape with $\mathcal{A} = 3.676$, when subjected to charges $Q = 5.78\pi$ and 5.79π. The figure gives evidence of the charge lost value corrected up to two decimal places.

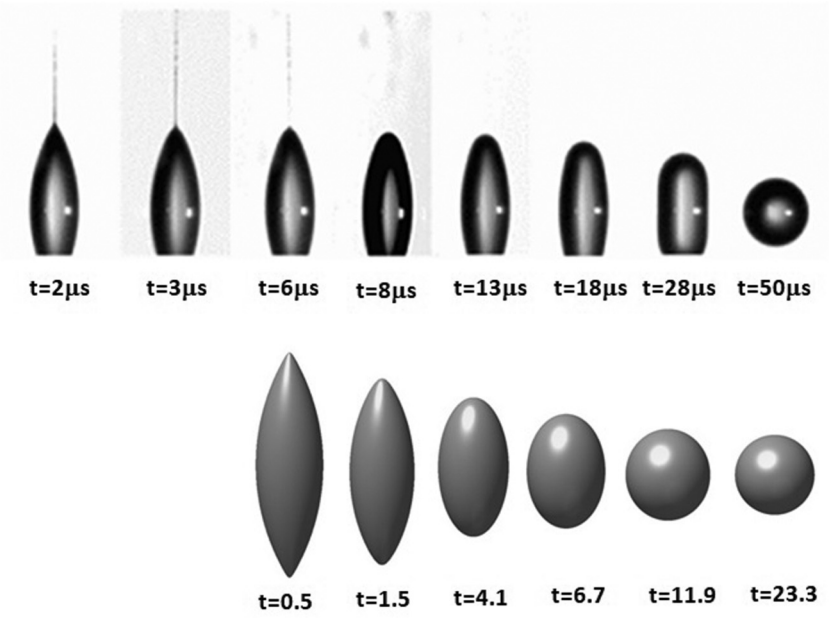

FIG. 9. Evolution of the drop in the relaxation regime from the critical shape, when subjected to charge $Q < 4.96\pi$. The drop shapes experimentally observed by Giglio *et al.* [25] (top) compare well with present simulations (bottom) and relaxation to a sphere can be observed.

of viscosity ratio $\lambda = 1$, analysis for $\lambda = 150$ (not presented here) shows drop regression almost at the same value of charge. This reemphasizes the fact that the viscosity ratio between the drop and the surrounding medium affects only the transient dynamics of the process but not the charge lost in the Rayleigh breakup.

In Fig. 9 we show the sequence of relaxation of the drop during its regressive regime obtained from simulations and compare it with the experimental snapshots reported by Giglio *et al.* [25]. A comparison of $\mathcal{A}$ as a function of normalized times in the relaxation regime, obtained from experimental and simulation results, is shown in Fig. 10. In our simulations, the drop relaxes back monotonically to the shape of a sphere due to the presence of viscous damping, unlike the case of the previous study [25] where it oscillates due to an inviscid assumption. As our numerical scheme could not capture the events occurring during actual jet ejection, the comparison is made only for the postejection experimental scenario. Qualitative agreement between the simulated and the experimental results on the transient history of the AR can be clearly seen. Any further comparative analysis can only be carried out by simulating the jet ejection stage, which requires a more efficient numerical algorithm that can continue after the formation of singular shapes.

IV. CONCLUSION

This study addressed the question of charge loss due to Rayleigh fission of a viscous liquid drop from a numerical perspective using boundary-element methods. The deformation dynamics up to the point of singularity corresponding to the onset jet ejection and the subsequent dynamics of relaxation back into the spherical shape were presented. A maximum aspect ratio of about 3.86 was obtained for the shape near its point of breakup (singularity), for viscosity ratio $\lambda = 150$. This is in agreement with the value (3.85) observed in the experimental images of drops ejecting Rayleigh jets, available in the literature [25]. As the code breaks down near the point of jet ejection due to the occurrence of shape singularity, the critical point was obtained using scaling laws and best-fit analysis. Further,

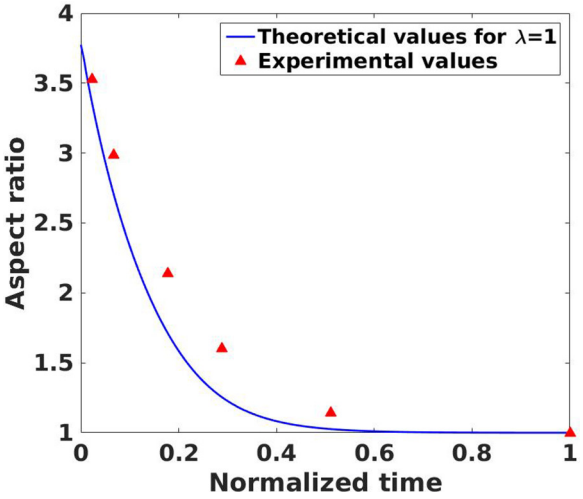

FIG. 10. Variation of aspect ratio with respect to self-normalized time for the case $\lambda = 1$ and their comparison with the experimental results reported by Giglio *et al.* [25] in the relaxation regime.

the charge loss was estimated as the difference between the Rayleigh charge and the maximum charge that just stabilizes a deformed drop near the singular point. The simulations predicted the charge loss of about 39%, which is well within the range of experimental values reported in the literature [13–19]. The simulations also revealed the importance of the viscous stresses along with the curvature stress as a drop approaches a critical shape. The study not only advances our understanding of the progression-regression dynamics of the charged drops undergoing Rayleigh fission, but also suggests an approach to overcome the numerical challenge of predicting the associated charge loss.

[1] D. Duft, T. Achtzehn, R. Müller, B. A. Huber, and T. Leisner, Coulomb fission: Rayleigh jets from levitated microdroplets, Nature (London) **421**, 128 (2003).
[2] J. Zeleny, Instability of electrified liquid surfaces, Phys. Rev. **10**, 1 (1917).
[3] G. Taylor, Disintegration of water drops in an electric field, Proc. R. Soc. London Ser. A, Math. Phys. Sci. **280**, 383 (1964).
[4] N. Arya, S. Chakraborty, N. Dube, and D. S. Katti, Electrospraying: A facile technique for synthesis of chitosan-based micro/nanospheres for drug delivery applications, J. Biomed. Mater. Res. **88B**, 17 (2009).
[5] S. K. Cho, H. Moon, and C.-J. Kim, Creating, transporting, cutting, and merging liquid droplets by electrowetting-based actuation for digital microfluidic circuits, J. Microelectromech. Syst. **12**, 70 (2003).
[6] P. Kebarle, A brief overview of the present status of the mechanisms involved in electrospray mass spectrometry, J. Mass Spectrom. **35**, 804 (2000).
[7] R. G. Cooks, Z. Ouyang, Z. Takats, and J. M. Wiseman, Ambient mass spectrometry, Science **311**, 1566 (2006).
[8] R. L. Grimm and J. L. Beauchamp, Dynamics of field-induced droplet ionization: Time-resolved studies of distortion, jetting, and progeny formation from charged and neutral methanol droplets exposed to strong electric fields, J. Phys. Chem. B **109**, 8244 (2005).
[9] E. Lac and G. M. Homsy, Axisymmetric deformation and stability of a viscous drop in a steady electric field, J. Fluid Mech. **590**, 239 (2007).
[10] R. T. Collins, M. T. Harris, and O. A. Basaran, Breakup of electrified jets, J. Fluid Mech. **588**, 75 (2007).

[11] W. Gu, P. E. Heil, H. Choi, and K. Kim, Comprehensive model for fine Coulomb fission of liquid droplets charged to Rayleigh limit, Appl. Phys. Lett. **91**, 064104 (2007).
[12] L. Rayleigh, On the equilibrium of liquid conducting masses charged with electricity, Philos. Mag. **14**, 184 (1882).
[13] A. Doyle, D. R. Moffett, and B. Vonnegut, Behavior of evaporating electrically charged droplets, J. Colloid Sci. **19**, 136 (1964).
[14] M. A. Abbas and J. Latham, The instability of evaporating charged drops, J. Fluid Mech. **30**, 663 (1967).
[15] J. W. Schweizer and D. N. Hanson, Stability limit of charged drops, J. Colloid Interface Sci. **35**, 417 (1971).
[16] M. Roulleau and M. Desbois, Study of evaporation and instability of charged water droplets, J. Atmos. Sci. **29**, 565 (1972).
[17] D. C. Taflin, T. L. Ward, and E. J. Davis, Electrified droplet fission and the Rayleigh limit, Langmuir **5**, 376 (1989).
[18] C. B. Richardson, A. L. Pigg, and R. L. Hightower, On the stability limit of charged droplets, Proc. R. Soc. London Ser. A, Math. Phys. Sci. **422**, 319 (1989).
[19] J. S. Shrimpton, Dielectric charged drop break-up at sub-Rayleigh limit conditions, IEEE Trans. Dielectr. Electr. Insul. **12**, 573 (2005).
[20] S. I. Betelú, M. A. Fontelos, U. Kindelán, and O. Vantzos, Singularities on charged viscous droplets, Phys. Fluids **18**, 051706 (2006).
[21] J. C. Burton and P. Taborek, Simulations of Coulombic Fission of Charged Inviscid Drops, Phys. Rev. Lett. **106**, 144501 (2011).
[22] R. T. Collins, K. Sambath, M. T. Harris, and O. A. Basaran, Universal scaling laws for the disintegration of electrified drops, Proc. Natl. Acad. Sci. USA **110**, 4905 (2013).
[23] M. Garzon, L. J. Gray, and J. A. Sethian, Numerical simulations of electrostatically driven jets from nonviscous droplets, Phys. Rev. E **89**, 033011 (2014).
[24] A. J. Radcliffe, Non-conforming finite elements for axisymmetric charged droplet deformation dynamics and Coulomb explosions, Int. J. Numer. Methods Fluids **71**, 249 (2013).
[25] E. Giglio, B. Gervais, J. Rangama, B. Manil, B. A. Huber, D. Duft, R. Müller, T. Leisner, and C. Guet, Shape deformations of surface-charged microdroplets, Phys. Rev. E **77**, 036319 (2008).
[26] J. D. Sherwood, Breakup of fluid droplets in electric and magnetic fields, J. Fluid Mech. **188**, 133 (1988).
[27] C. Pozrikidis, *Boundary Integral and Singularity Methods for Linearized Viscous Flow* (Cambridge University Press, Cambridge, 1992).
[28] O. A. Basaran and L. E. Scriven, Axisymmetric shapes and stability of isolated charged drops, Phys. Fluids A **1**, 795 (1989).
[29] S. D. Deshmukh and R. M. Thaokar, Deformation, breakup and motion of a perfect dielectric drop in a quadrupole electric field, Phys. Fluids **24**, 032105 (2012).
[30] S. Das, Y. S. Mayya, and R. Thaokar, Dynamics of a charged drop in a quadrupole electric field, Europhys. Lett. **111**, 24006 (2015).
[31] J. D. Jackson, *Classical Electrodynamics* (Wiley, New York, 2007).